The Resilience and Vulnerability of Human Brain Networks Across the Lifespan

Pin Shu, Hong Zhu, Wen Jin, Jie Zhou, Shanbao Tong, *Senior Member, IEEE*, and Junfeng Sun, *Senior Member, IEEE*

***Abstract*— Resilience, the ability for a system to maintain its basic functionality when suffering from lesions, is a critical property for human brain, especially in the brain aging process. This study adopted a novel metric of network resilience, the Resilience Index (RI), to assess human brain resilience with three different lifespan datasets. Based on the structural brain networks constructed from diffusion tensor imaging (DTI), we observed an inverted-U relationship between RI and age, that is, RI increased during development and early adulthood, reached a peak at about 35 years old, and then decreased during aging, which suggested that brain resilience could be quantified by RI. Furthermore, we studied brain network vulnerability by the decreases in RI when virtual lesions occurred to nodes (i.e., brain regions) or edges (i.e., structural brain connectivity). We found that the strong edges were markedly vulnerable, and the homotopic edges were the most prominent representatives of vulnerable edges. In other words, an arbitrary attack on homotopic edges would have a high probability to degrade brain network resilience. These findings suggest the change of human brain resilience across the lifespan and provide a new perspective for exploring human brain vulnerability.**

***Index Terms*— Brain network resilience, diffusion tensor imaging, homotopic edges, lifespan, vulnerability.**

I. Introduction

THE ability that brain could withstand lesions and maintain its basic functionality is called brain resilience. It seems that the effects of lesions in different locations have no unequivocal pattern: some lesions bring negligible effects [1], [2], while some relatively small lesions may have broad, even irreversible effects [3]–[8]. Therefore, the resilience and vulnerability of human brain networks is worthy of research and has motivated numerous empirical and computational studies [9], [10].

Complex network analysis considers brain as a network, where network 'nodes' refer to brain regions and 'edges' describe the connectivity between brain regions [11], [12]. In such a network, the vulnerable nodes or edges are defined by the significant lesion effects when they are damaged. With the development of large-scale brain connectivity maps (both structural and functional) and computational models [11], [13]–[15], quite a few studies have explored the lesion effects on brain functionality and identified the vulnerable nodes or edges. The usual method was to simulate the brain activity using a large-scale dynamics model, and virtually lesion the structural connectivity (referring to neural fibers between brain regions) in the model. The lesion effect could subsequently be assessed by the difference between the simulated functional connectivity (referring the statistical association between the representative functional signals for brain regions) with virtual lesions and the one without virtual lesions. Based on this research framework, several studies showed that lesion effects might depend on the topological and anatomical features of the lesion site. For example, Vasa *et al.* found that the lesions of regions with high centrality resulted in the most significant decrease in functional performance, indicating that brain is not resilient to attacks on hubs [16]. Besides, Alstott *et al.* reported that lesions along the cortical midline, the temporoparietal junction and the frontal cortex impacted most on functional connectivity [17]. All the studies attempted to point out the sites where lesions would result in severe effects on brain, which may offer guidance for clinical interventions.

However, despite various computational models to simulate the neural activity of brain, the neural dynamics is still not well illuminated at the system level [18], and the function that could appropriately represent human brain state remains to be explored. In 2016, Gao and his colleagues proposed a universal index, which could evaluate a system's resilience without its dynamic model and simulated functional connectivity, but only with its structural connectivity [19]. They found that perturbations on the structural connectivity would affect a system's resilience by changing its activities. Resilience Index (RI), a metric which simultaneously captures density, heterogeneity, and symmetry of structural networks, was proved to universally play a significant role in regulating network

Manuscript received March 31, 2021; revised June 11, 2021; accepted July 5, 2021. Date of publication August 19, 2021; date of current version September 3, 2021. This work was supported in part by the National Natural Science Foundation of China under Grant 61673267, Grant 61976136, and Grant U20B2074; in part by the Science and Technology Commission of Shanghai Municipality under Grant 19441907900; in part by Shanghai Key Laboratory of Psychotic Disorders Open Grant 18-K03; and in part by the Key Project of Translational Medicine Fund of Shanghai Jiao Tong University under Grant ZH2018ZDA30. *(Pin Shu and Hong Zhu contributed equally to this work.) (Corresponding author: Junfeng Sun.)*

This work involved human subjects or animals in its research. Approval of all ethical and experimental procedures and protocols was granted by the Cambridge Centre for Ageing and Neuroscience, the Consortium for Reliability and Reproducibility, and the Nathan Kline Institute-Rockland Sample.

The authors are with the School of Biomedical Engineering, Shanghai Jiao Tong University, Shanghai 200240, China (e-mail: jfsun@sjtu.edu.cn).

This article has supplementary downloadable material available at https://doi.org/10.1109/TNSRE.2021.3105991, provided by the authors.

Digital Object Identifier 10.1109/TNSRE.2021.3105991

resilience in multiple fields including the noise system [20], ecological system [21], and power supply system [19]. Both the theoretical derivation and empirical results indicate that larger RI can generally indicate higher resilience for one system. With this framework of resilience, then in principle, the structural metric RI could be employed to infer whether a system is resilient and further help to quantify the effects of structure lesions in different sites.

In the present study, we adopted the Resilience Index to assess human brain network resilience, which refers to the ability that brain withstands lesions. Based on three different public lifespan datasets, we investigated the relationship between RI and age. Since the specific inverted-U shape trajectories exist for various cognitive, functional, and structural measures regarding the development and aging of human brain [22]–[26], we assumed that the age trajectory may tell whether RI is applicable to assess human brain resilience. If RI could quantify human brain resilience, the decrease of RI induced by a virtual lesion seems to be a nice indicator of the lesion effect, thus helping to identify the vulnerable nodes or edges. This study aimed to explore vulnerable areas without dynamic models but with a novel metric of network resilience, offering a new window into how brain structure impacts on its functionality.

II. Materials and Method

A. Datasets

This study involved three public datasets. The first dataset was from the Cambridge Centre for Ageing and Neuroscience (*Cam-CAN,* http://www.cam-can.com) [27]. In total, the data of 627 healthy participants were downloaded, and two participants lacking T1 images or DTI images were excluded in this study. All the MRI data were scanned at a single site using a 3T Siemens TIM Trio scanner. T1 images were acquired using 3D MPRAGE sequence, TR = 2250 ms, TE = 2.99 ms, TI = 900 ms, flip angle = 9 deg, FOV = 256 × 240 × 192 mm, voxel size = 1 mm isotropic. DTI images were acquired using Twice-Refocused SE sequence, TR = 9100 ms, TE = 104 ms, FOV = 192 × 192 mm, voxel size = 2 mm isotropic.

The second dataset was from Consortium for Reliability and Reproducibility(CoRR, http://fcon_1000.projects.nitrc.org/indi/CoRR/html/data_citation.html) [28]. The CoRR dataset includes 33 datasets, among which most datasets were collected from participants in narrow age range. In this study, the data of 74 participants was downloaded from four lifespan datasets (i.e., IPCAS8, MRN, NYU2, and XHCUMS) of the CoRR dataset.

The third dataset was from the enhanced Nathan Kline Institute-Rockland Sample (NKI-RS, http://fcon_1000.projects. nitrc.org/indi/enhanced/index.html) [29]. In total, the data of 349 participants were downloaded, among which 140 participants with $b_0 = 0$ were selected. Unlike the previous datasets, this heterogeneous dataset included 76 healthy participants and 64 participants with various mental disorders like depression and anxiety.

All the three datasets were downloaded and used with permission and under the regulation proposed by data providers.

TABLE I
The Demographic Information of the Three Datasets

Dataset	Cam-CAN	CoRR	NKI-RS
Sample Size	625	74	140
Age (years)	18 - 88	6 - 62	7 - 83
Gender (Female/Male)	316/309	33/41	74/66
Sample Characteristics	Healthy participants	Healthy participants	Healthy participants and participants with mental disorders

The basic demographic information of the selected data from these three datasets was given in Table I. In this study, the CoRR dataset and the NKI-RS dataset were used to validate the results of the Cam-CAN dataset.

B. Data Preprocessing and Network Construction

Data preprocessing and network construction were carried out using Pipeline for Analyzing braiN Diffusion imAges toolbox [30]. The toolbox was mainly based on packages like FSL (http://fsl.fmrib.ox.ac.uk/fsl/fslwiki/) and Diffusion Toolkit (https://www.nitrc.org/projects/trackvis/). First, the b_0 image without diffusion weighting was employed to estimate the brain mask, which could help to crop the raw images and correct for the eddy-current effect [31]. Then, the brain was divided into 90 regions based on the Automated Anatomical Labeling brain atlas (AAL90, see details in Supplementary Table. SIV), and each region was defined as one node for the structural brain network. Finally, network construction was performed using deterministic tractography. Fiber tracts were tracked by seeding from all the white matter voxels unless the fractional anisotropy (FA) < 0.2 or bending angle $> 45°$. The structural connectivity (SC) was eventually constructed, and the edge strength was caculated as the average FA value of neural fibers that linked the two corresponding brain regions. Here, we chose FA values to investigate the relationship between white matter tracts and age according to some relevant studies [32]–[36].

C. Resilience Index and Its Components

The traditional framework of resilience designed for systems containing one element employs a universal equation to describe their behavior [37], [38]:

$$\frac{dx}{dt} = f(x, \beta), \tag{1}$$

where x refers to the element's state, defined as the magnitude of activity at a single time point; β reflects the changing conditions, and $f(x, \beta)$ refers to the system's dynamics. Assuming that the system could be in a steady state x_0, then we have [38]:

$$f(x_0, \beta) = 0, \tag{2}$$

$$\frac{\partial f}{\partial x}|_{x=x_0} < 0, \tag{3}$$

where Equation (3) guarantees the linear stability at the fixed point x_0. Given a specific β, if the system has one and only

one fixed point x_0, it is at a stable state; if the system has no fixed point or more than one fixed points, it is at an unstable state. Since β could regulate system state, if its value is far away from the critical β^c, it could keep a system from losing its stability.

For a high-dimensional system consisting of N variables with states $\boldsymbol{x} = (x_1, x_2, \ldots, x_N)^{\mathrm{T}}$, it could be characterized by the following dynamic coupled equation:

$$\frac{dx_i}{dt} = F(x_i) + \sum_{j=1}^{N} A_{ij} G(x_i, x_j), \tag{4}$$

where $F(x_i)$ and $\mathrm{G}(x_i, x_j)$ capture the dynamics of single variable x_i and the coupling between variables x_i and x_j. The behavior of the high-dimensional system could not be regulated by a single parameter β but by its connection matrix A_{ij}. Gao *et al.* proposed a framework to reduce its dimensionality to one-D by mathematical transformations [19], and gained the equation with a similar form of Equation (1):

$$\frac{dx_{eff}}{dt} = F(x_{eff}) + \beta_{eff} G(x_{eff}, x_{eff}), \tag{5}$$

where β_{eff} is abstracted from the network connection matrix A_{ij} by

$$\beta_{eff} = \frac{< s^{out} s^{in} >}{< s >}, \tag{6}$$

in which $s^{out} = (s_1^{out}, \ldots, s_N^{out})^T$ is the vector of outgoing weighted degrees and $s^{in} = (s_1^{in}, \ldots, s_N^{in})^T$ is the vector of incoming weighted degree, $< s >=< s^{in} >=< s^{out} >$ is the average weighted degree, s_i^{out} and s_i^{in} $(1 \le i \le N)$ are the outgoing degree and incoming degree of the ith node (variable). β_{eff} plays a role in high-dimensional systems just like β in one-dimensional systems.

We assessed brain network resilience based on a Resilience Index (RI) proposed by Gao and his colleagues [19]. Both the theoretical derivation and empirical results indicate that a larger β_{eff} generally represents higher resilience for one system [19]. In this study, we would use β_{eff} defined in Equation (6) as RI. For an undirected network, the degree of a node is defined as the number of edges connected to it, and the strength of a node is defined as the sum of the weights of all edges connected to it. For a directed network, outgoing weighted degree and incoming weighted degree of a node are defined as the sum of the weights of all outgoing edges from the node and the sum of the weights of all incoming edges to the node respectively. In this study, considering that the structural brain network is undirected, RI for bra+in can be calculated as:

$$RI = \frac{< s \cdot s >}{< s >}. \tag{7}$$

Besides, Gao and his colleagues demonstrated that RI can be written as the sum of two network topological features (Fig. 1):

$$RI =< s > + H, \tag{8}$$

where $< s >$ is the average of all node strength and reflects network density, and $H = \sigma^2 / < s >$ represents network heterogeneity, in which σ is the variance of all node strength.

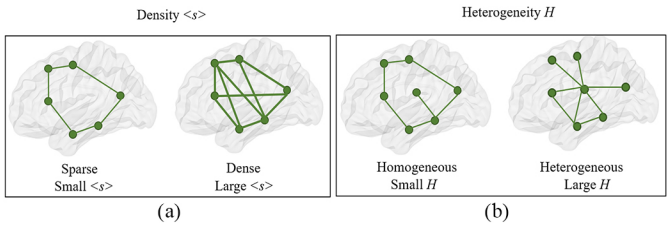

Fig. 1. Demonstration of the two topological features, i.e., density $< s >$ (a) and heterogeneity H (b), of network that determine Resilience Index.

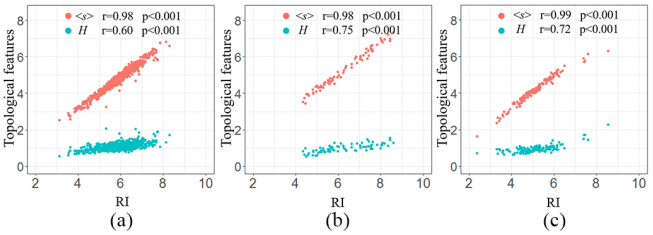

Fig. 2. Scatter plots of two topological features (Density $< s >$ and Heterogeneity H) with respect to RI in the Cam-CAN (a), CoRR (b), and NKI-RS (c) datasets, respectively. The Pearson's correlation coefficients r and p-values between RI and $< s >$ or H are provided, respectively.

D. Statistical Analysis

We tried both the linear model and quadratic model to fit the age trajectory of RI, following previous studies that generally used these models to examine the relationships between age and other structural network measures [39], [40]. Here, R-square, the proportion of variability in a dataset that is accounted for by the statistical model, was employed to assess the goodness-of-fit. The R-square values (Table SI) told that data could be explained better by the quadratic model than the linear model. Therefore, we performed binomial fitting regression analyses to evaluate the age effect of the RI.

Besides, we calculated the topological features of the structural connectivity matrix using the Brain Connectivity Toolbox (BCT) [41]. All calculation was implemented using Matlab (version 2014a; MathWorks) and visualization of results were performed using RStudio.

III. Results

A. The Relationships Between RI and Network Density or Heterogeneity

According to Equation (8), RI of the structural brain network was determined by two global topological features, i.e., network density $< s >$ and network heterogeneity H. As shown in Fig. 2, network density $< s >$ accounted for a larger proportion of RI than network heterogeneity H. Besides, the correlation coefficients between RI and $< s >$ approximated to 1 in all the three datasets (Cam-CAN: 0.98; CoRR: 0.98; NKI-RS: 0.99); while the correlation coefficients between RI and H were relatively lower (Cam-CAN: 0.60; CoRR: 0.75; NKI-RS: 0.72).

B. The Relationship Between RI and Age

We examined the relationship between RI and age. Results showed that RI had a quadratic relationship with age (Fig. 3).

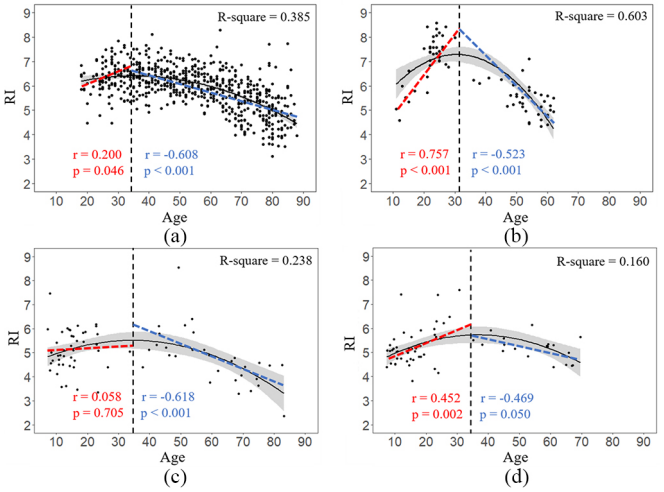

Fig. 3. The relationships between RI and age in the Cam-CAN dataset (a), the CoRR dataset (b), the cohort of healthy participants (c) and the cohort of patients (d) from the NKI-RS dataset. Each dot represents one participant, and a quadratic fitting regression line with 95% confidence interval (shading area) is illustrated for each case. The black dash lines indicate the corresponding age where the fitting curves reach peaks respectively, and divide the participants into two parts (i.e., adolescence and early adulthood, middle and later adulthood) for the four datasets respectively. The red trend lines are linear regression lines for the adolescence and early adulthood; the blue trend lines are linear regression lines for the middle and later adulthood. The Pearson's correlation coefficients r, p values and R-square values (quadratic fitting) are provided, respectively.

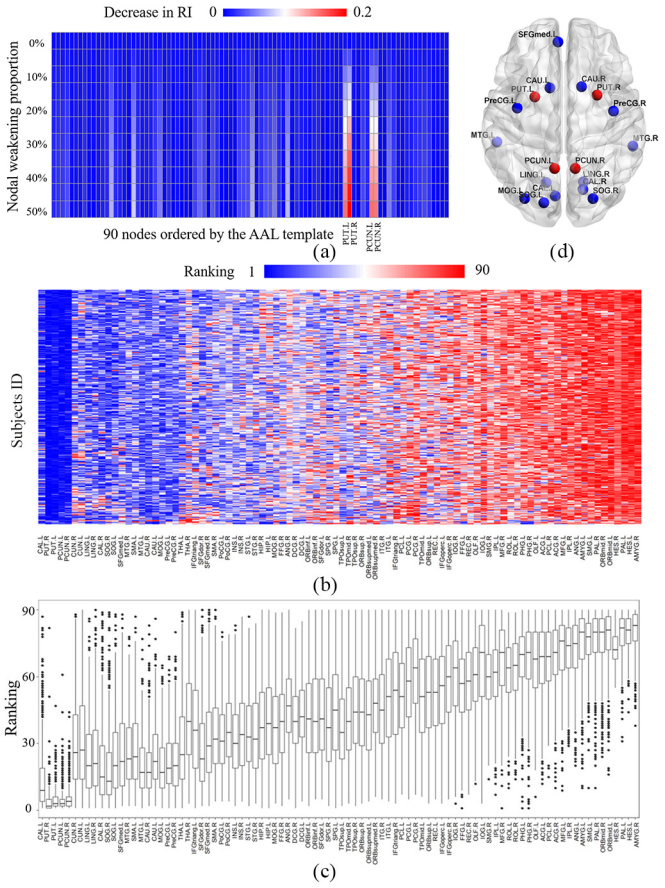

Fig. 4. Impacts of the 90 nodes on RI for participants from the Cam-CAN dataset. (a) The heat map showed that RI decreased with the increase of nodal weakening proportion for all 90 nodes respectively for one typical participant. (b) The clustering heat map of the rankings of 90 nodes for all 625 participants from the Cam-CAN dataset. (c) The boxplot of the rankings of 90 nodes respectively for all 625 participants. Black dots denote the outliers which are not in the range from the lower quartile minus 1.5 times of interquartile range to the upper quartile plus 1.5 times of interquartile range. (d) The spatial location of the top 20% ranked nodes (blue, the top 4 nodes are colored in red) in the AAL template.

Here, R-square, the proportion of variability in a dataset that is explained by the statistical model, was employed to assess the goodness-of-fit. For the Cam-CAN dataset (Fig. 3(a)), the inverted-U curve captured RIs of the healthy participants from 18 to 88 years old, reaching the peak at about 35 years old (R-square=0.385). Here, the inflexion point was determined by the top of the quadratic fitting curve. Before the peak, RI was significantly positively correlated with age ($p=0.046$); after the peak, RI was significantly negatively correlated with age ($p<0.001$). The similar inverted-U quadratic relationship between RI and age also appeared in the CoRR dataset (Fig. 3(b), peak appeared at 31 years old), the cohort of healthy participants in the NKI-RS dataset (Fig. 3(c), peak appeared at 34 years old) and the cohort of patients in the NKI-RS dataset (Fig. 3(d), peak appeared at 35 years old). The inverted-U curves suggested that RI of the brain network increases during development and early adulthood, then reaches a peak at about 35 years old, and finally decreases during the aging process. Also, for the NKI-RS dataset, we found that mental disorders had no significant impact on the age-related RI values by using a general linear model (Supplementary Table. SV). So, the data of 140 participants from the NKI-RS were analyzed as a whole hereafter.

C. Impacts of Nodes on RI

We investigated the impacts of the 90 defined nodes (i.e., 90 AAL ROIs) on RI. For each node, we simulated damage of different levels on it by proportionally reducing the strength (from 0% to 50%) of all the edges connected it. Results showed that RI decreased with increasing nodal damage (Fig. 4(a)). For some nodes, such as bilateral putamens (PUT.L and PUT.R) and precuneus (PCUN.L and PCUN.R), simulated damage on them resulted in larger decreases in RI than on other nodes. Further, according to the decrease in RI with the 50% nodal weakening, 90 nodes were ranked from 1 to 90. It meant that damage on the node ranking first would lead to the largest decrease in RI. To compare the rankings of ROIs across all participants, we conducted a clustering analysis, which can simultaneously reveal row (participants) and column (ROIs) hierarchical cluster structure in a data matrix [42]. As shown in the clustering heat map (Fig. 4(b)) and average ranking (Fig. 4(c)), PUT.R, PUT.L, PCUN.R, PCUN.L showed the highest ranking among all 625 participants consistently. Besides, Fig. 4(d) illustrated the top 20% ranked nodes, most of which were symmetrically distributed in the bilateral brain hemispheres.

We also examined the effects of age and gender on RI by a general linear model, and found that age and gender had

significant impacts on RI (Supplementary Table SIII). After adjusting the effects of age and gender, we recalculated the impacts of weakening node on RI, and found that the nodal rankings were similar with those before adjusting the effects of age and gender (Supplementary Fig. S1).

D. Impacts of Edges on RI

We investigated the impacts of edges on RI with seven strategies of attack simulations. The first strategy was to eliminate the strongest edges by the order. The second strategy was to eliminate the weakest edges by the order. These two strategies were employed to examine how the strength of edges contribute to RI. The third strategy was to eliminate edges randomly. The fourth strategy was to randomly delete the homotopic edges (edges that link two geometrically symmetrical regions, see red edges in Fig. 7(a)). The fifth strategy was to randomly delete the other inter-hemispheric edges (edges that link two nodes in two hemispheres respectively, see green edges in Fig. 7(a)) other than the homotopic ones. The sixth strategy was to randomly delete the intra-hemispheric edges (edges that link two nodes both within the left or the right hemisphere, see blue edges in Fig. 7(a)). These last three strategies aimed to explore the contribution of the edges with specific spatial embedding features to RI. Especially, we took the seventh strategy, i.e., deleting the edges connected with the temporal lobe hubs, which were reported to be associated with higher lesion probability in Alzheimer's disease [1].

The results showed that, among the first six strategies, deleting the strongest edges (i.e., strategy 1) resulted in the largest decrease of RI, while deleting the weakest edges (i.e., strategy 2) resulted in the smallest decrease of RI. Randomly deleting edges (i.e., strategy 3) resulted in a medium decrease between strategy 1 and strategy 2 (Figs. 5(a) and 5(b)). Furthermore, deleting the homotopic edges (i.e., strategy 4) and other inter-hemispheric edges (i.e., strategy 5) resulted in a greater decrease of RI than the case of deleting intra-hemispheric edges (i.e., strategy 6) (Figs. 5(c) and 5(d)). These results suggested that edges with high strength or inter-hemispheric embedding have large impacts on RI. What's more, deleting the edges connected with the temporal lobe hubs (i.e., strategy 7) resulted in similar decrease of RI with deleting homotopic ones (i.e., strategy 4) (Fig. 5(d)). We also investigated the impacts of edges on RI with the seven strategies of simulated attacks after adjusting the effects of age and gender by a general linear model, and found similar results as those before adjusting the effects of age and gender (Supplementary Fig. S2).

We further examined the relationship between the strongest edges and age. For each edge, it may be one of the strongest edges for some participants but not for other participants, so if its strength ranked top i for more than 30% of all participants, we would take it into the representative set D_i, as the strongest edges of group. We summed up the strength of edges in D_i for each participant and found that it also had a quadratic relationship with age (Fig. 6(c)). The goodness of quadratic fitting was then evaluated by R-square. Results showed that R-square value increased to saturation and fluctuated within

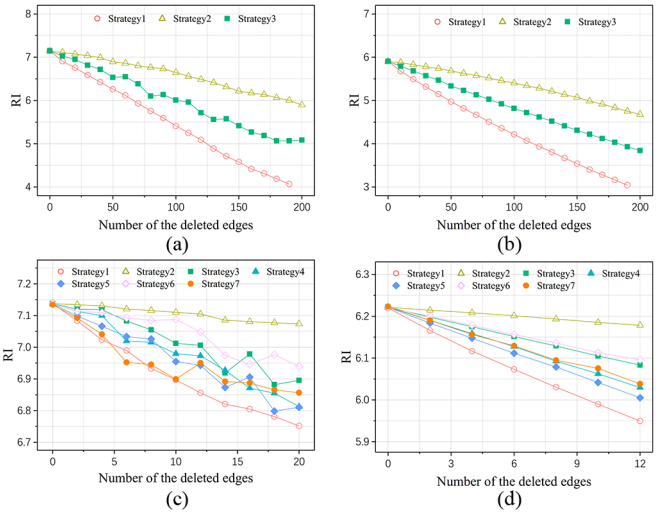

Fig. 5. Impacts of removing edges on RI under seven strategies of random errors or targeted attacks for participants from the Cam-CAN dataset. Strategy 1 refers to deleting the strongest edges, strategy 2 refers to deleting the weakest edges, strategy 3 refers to randomly deleting edges, strategy 4 refers to deleting the homotopic edges; strategy 5 refers to deleting other inter-hemispheric edges except homotopic ones; strategy 6 refers to deleting intra-hemispheric edges; and strategy 7 refers to deleting the edges connected with the temporal lobe hubs. (a) The RI of one typical participant with respect to the number of edges deleted (up to 200) under the first three strategies. The maximum number of edges we can delete here was determined by the minimum number (i.e., 210 for the Cam-CAN dataset) of non-zeros edges among all participants and we deleted up to 200 edges eventually for illustrations purpose. (b) The average RI of all the 625 participants with respect to the number of edges deleted (up to 200) under the first three strategies. (c) The RI of one typical participant with respect to the number of edges deleted under the seven strategies. Note that the maximum number of deleted edges here was determined by the number of homotopic edges in this typical participant, that is, this participant has only 20 homotopic edges. (d) The average RI of 438 participants with respect to the number of edges deleted under the seven strategies. Here these selected 438 participants all have 12 or more homotopic edges.

a narrow range (Fig. 6(a)). We empirically set the saturation threshold at 0.5 and got 86 edges (Fig. 6(b)). The total strength of these 86 edges was suggested to have a best inverted-U relationship with age (Fig. 6(c)). To eliminate the possibility of coincidence, we randomly picked 86 edges from all edges (546 edges) which existed in more than 30% of all participants and calculated the R-square values. The procedure was repeated 100,000 times. The frequency histogram told that 0.5 ranked top 0.01% among all the 100,000 R-square values (Fig. 6(d)). Since theses strongest edges have great impacts on RI (Fig. 5(c)) and their total strength have an inverted-U relationship with age, which is similar with the relationship between RI and age, we would call the so defined top edges as 'resilience-related' edges hereafter. Note that similar results under thresholds other than 30% have also been found (see details in Supplementary Fig. S3).

E. Spatial Embedding Feature of the "Resilience-Related" Edges

Regarding the spatial embedding feature, the 86 strongest edges were classified into three types: 13 homotopic edges, 52 inter-hemispheric edges and 21 intra-hemispheric

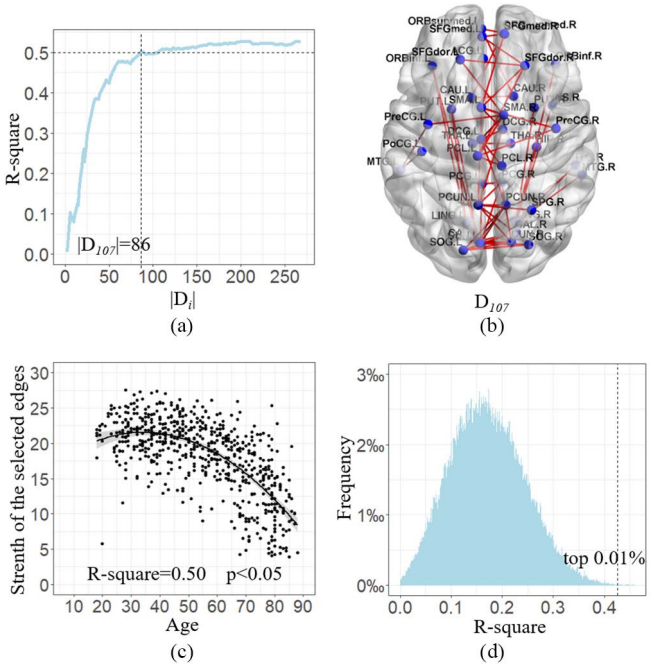

Fig. 6. The inverted-U relationship between age and the strongest edges. (a) The goodness-of-fit (indicated by R-square value) changed with the potential of D_i ($1 \leq i \leq 236$), i.e., the number of edges in the representative set D_i of group top edges ($|D_i|$). The value of R-square almost stabilized around 0.5 when $|D_i| > 86$, here $i = 107$. (b) The top 86 edges in D_{107}. (c) The relationship between age and the sum of the strength of the 86 strongest edges was captured by the quadratic fitting regression line with 95% confidence interval (shading area). (d) Histogram of R-square values for the 100000 times of randomly picked 86 edges from all possible edges (546 edges) existing in more than 30% of all participants. The vertical dash line indicates the R-square value of the top 0.01%.

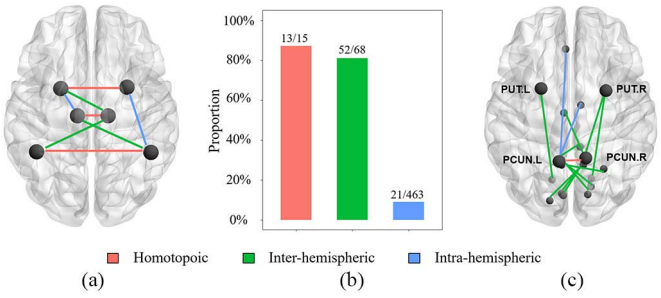

Fig. 7. Spatial embedding feature of the 'resilience-related' edges. (a) Illustration of the three types of edges, i.e., homotopic edges, inter-hemispheric edges and intra-hemispheric edges according to the spatial location of the two nodes they connect. (b) The numbers of the three types of edges (i.e., 13, 52, and 21 respectively) in the picked 86 'resilience-related' edges and the corresponding numbers of the three types of edges (15, 68, and 463 respectively) for all the possible 546 edges in brain networks. (c) 14 'resilience-related' edges connected with PUT.L, PUT.R, PCUN.L and PCUN.R.

edges (Fig. 7(a)). Normalized by their corresponding number of edges in all the 546 possible edges, we found that the proportion of the intra-hemispheric edges was far smaller than that of the other two types of edges (Fig. 7(b)). Besides, among the 84 'resilience-related' edges, 14 edges connected with PUT.L, PUT.R, PCUN.L and PCUN.R (Fig. 7(c)), which were observed to have the greatest impacts on RI (Fig. 4).

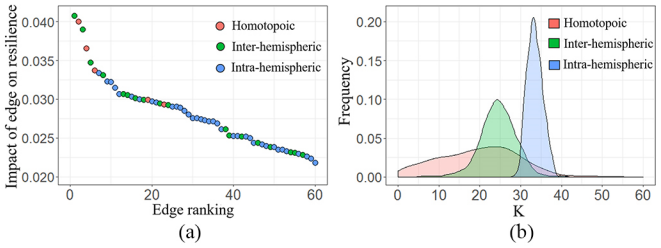

Fig. 8. Impacts of different spatial embedding edges on RI. (a) For one typical participant, the 80 edges inducing the largest deceases in RI and their respective types. (b) The frequency distributions of K. For the jth type of edge, K denotes the value of K_j calculated by equation (9), which is the average rankings of one type of edge in the top 80 ranking edges for all 625 participants.

We further assessed the impacts of different spatial embedding edges at the individual level besides the group level. For one participant, we firstly calculated the decrease in RI after eliminating each edge. Then we picked the 80 edges that induced the largest decreases in RI and ranked them in descending order. To quantify the average ranking for each edge type (homotopic, inter-hemispheric, and intra-hemispheric) among the top 80 edges, K_j was defined as:

$$K_j = \frac{\sum_{i=1}^{80} \mathbf{1}\left(e_i \in C_j\right) \cdot i}{\sum_{i=1}^{80} \mathbf{1}\left(e_i \in C_j\right)}, \tag{9}$$

where C_j denotes the jth type of edge, i denotes the ranking of edge e_i, $\mathbf{1}(\cdot)$ is the indicator function which equals 1 or 0 when $(\cdot)$ is true or false respectively. The frequency distributions of K_j $(j = 1, 2, 3)$ for all the 625 participants demonstrated that in general, the homotopic edges had the highest average ranking while the intra-hemispheric edges had the lowest average ranking (Fig. 8(b)). Note that similar results have also been observed in the top 60, 70, 90 and 100 ranking edges (see details in Supplementary Fig. S4).

IV. Discussion

Overall, this study explored the resilience and vulnerability of human brain networks across the lifespan with a novel measurement of network resilience, the Resilience Index (RI). We observed an inverted-U relationship between RI and age, which provides evidence for our speculation that RI is applicable to quantify human brain resilience. Furthermore, we inferred the vulnerable nodes (e.g., bi-hemispheric putamens and precuneus) and edges (i.e., inter-hemispheric edges and edges with high strength) by the significant decreases in RI when they were removed. Finally, we found that part of the strongest edges might be most related with resilience and thus referred them as 'resilience-related' edges. Among these 'resilience-related' edges, homotopic edges were the most prominent representatives. In other words, an arbitrary attack on homotopic edges would have a high probability to degrade brain network resilience.

A. Resilience Index as a Measurement of Brain Network Resilience

Most previous studies assessed brain lesion effects based on structural connectivity (SC), computational models, and

simulated functional connectivity (FC) [11], [13], [14]. The usual method was to simulate brain activity using a dynamics model and then virtually lesion SC, then lesion effects could be reflected in the alteration of FC in simulation. Such strategy attempts to replay the events during real brain lesions, helping to identify many vulnerable brain regions [16], [17]. However, since the neural dynamics is still not well illuminated at the system level, no computational neural model has been commonly accepted yet [18]. A recent study investigated the brain resilience via functional connections, and the drop in the largest connected component (LCC) after removing the nodes or edges from the brain network was recorded as a measure of the inferred damage [43]. This study proposed resilience metrics from a functional perspective and exploited the influence of environmental and genetic factors on brain resilience. Indeed, brain network resilience based on structural network remained rarely studied. In 2016, Gao and his colleagues found that, regardless of dynamics, perturbations on SC would affect one system's activities. They transformed a high-dimensional system to a one-dimensional system and proposed a so-called Resilience Index to quantify the system's resilience. RI is a one-dimensional metrics, which simultaneously captures density, heterogeneity, and symmetry of a structural network. It has been demonstrated that larger RI generally indicates higher resilience in multiple high-dimensional systems including the ecological system, gene regulation system and power supply system [19]–[21], [44]. To the best of our knowledge, this theoretical model hasn't been used in the study of human brain resilience, though the possibility of its application on neuronal networks and neuropsychology study has been discussed in terms of perspectives and future challenges [45].

In this study, for the first time, we applied RI to assess brain network resilience via structural connectivity. For the Cam-CAN dataset, we observed an inverted-U relationship between RI and age, that is, RI increased during development and early adulthood, reached a peak at 35 years old, and then decreased during aging (Fig. 3). We have also calculated RI based on a brain template with 246 regions [46] and observed similar inverted-U tendency and similar inflexion point (35 years old) (Supplementary Fig. S7), suggesting that the inverted-U age trajectory of RI is not sensitive to the parcellation of ROI. Furthermore, the CoRR and NKI-RS datasets also showed the inverted-U tendency for RI across the lifespan, which empirically matched the development and aging process of human brain. There were differences among the results of the three datasets. For example, the fitting curve of the CoRR dataset is higher than those of other datasets (Fig. 3). The reason may be due to that participants in the CoRR dataset are generally younger. Similar inverted-U tendencies have been reported in cognitive (e.g., memory, [23]), functional (functional flexibility, [47]) and structural (e.g., white matter hyperintensities, [39]) measures. Therefore, we speculated that RI could be a candidate measure for brain network resilience and this method is of certain generalization under different brain templates and datasets. Besides, we conducted a supplementary analysis about comparisons between RI and other network metrics including relative local efficiency (LE), relative global efficiency (GE), and small-worldness. The results suggested that RI was significantly positively correlated with LE and GE, but negatively correlated with small-worldness (Supplementary Fig. S5).

Since the structural brain network is undirected, the RI of the brain network actually refers to the sum of two network metrics, i.e., network density and network heterogeneity according to Equation (6). As we know, density and heterogeneity are two critical properties for the structural brain network, and they have been reported to associate with brain resilience in previous studies [48], [49]. Compared with network heterogeneity, network density accounted for a larger proportion of RI and had a higher correlation with RI (Fig. 2), suggesting its primary contribution to RI. The result also gave a hint about the different contributions of various nodes or edges to RI: strong nodes or edges tend to contribute more because they can help to enhance network density, which is the primary factor; weak nodes or edges also played a role as they can contribute to network heterogeneity, which is the secondary factor.

B. The Vulnerable Nodes and Edges

In this study, we identified the vulnerable nodes by the Resilience Index. Our results showed that the removing of PUT.R, PUT.L, PCUN.R, PCUN.L would result in a sharp decline in RI for almost all participants (Fig. 4 and Supplementary Fig. S6), suggesting that attacks on these four brain regions were most likely to degrade brain resilience. In previous studies, the vulnerable brain regions have been identified by the decreases in network metrics such as global efficiency, local efficiency and the size of the largest component when a fraction of nodes is removed [50], [51]. Despite the difference in methods, the four vulnerable brain regions identified by RI were accordant with the previous vulnerability study [52]. Specially, these four nodes were distributed in the geometrically symmetrical regions of the left and the right hemispheres, and the phenomenon of geometrically symmetrical locations were also observed in other nodes that had large impacts on RI (Fig. 4(d)). Besides, we calculated the vulnerability rank of 90 nodes for participants in the CoRR and NKI-RS datasets respectively (Supplementary Fig. S6), and found that 11 nodes, i.e., bi-hemispheric PUT, PCUN, SOG, CAL, PreCG and right-hemispheric LING, consistently ranked top 20 most vulnerable notes in all the three datasets. We referenced previous studies and found the identified vulnerable nodes have been reported to be affected in neurodegenerative diseases (Supplementary Table SVIII), which support the availability of RI in exploring brain resilience.

Previous studies reported that putamen is one of the hub nodes (most connected nodes) in structural brain networks [53] and the key part of striatum, which supports the integration of dopaminergic inputs and incoming information in limbic, cognitive and motor control circuits [54]. Besides, precuneus is a functional core of the default-mode network, which showed increased susceptibility to age-related change [55] and neurodegenerative disease [56]. Putamen has been shown to be affected in many neurodegenerative disorders, e.g., Parkinson's disease (PD) and Alzheimer's disease (AD) [57]. Zhao and his

colleagues reported that the patients in amnestic mild cognitive impairment showed significant decreased FA in precuneus region [36]. Besides, kartaci and his colleagues reported that lower FA in the precuneus white matter was associated with higher clinical disease severity, suggesting the high vulnerability of precuneus [58]. In this study, the identified most vulnerable nodes were accordant with both the empirical and computational studies. Although the vulnerability ranks of putamens and precuneus were consistently high among all three datasets, they have significant but opposite statistical correlation with age (Supplementary Table SIX). It means that precuneus may become more vulnerable with age while putamen may become less vulnerable with age. This result is quite interesting and needs to be explored in the subsequent work.

The vulnerable edges are another fundamental object in vulnerability studies. According to strength and spatial embedding feature, structural edges were classified to different types. Regarding the edge strength, the results of damage simulation showed that attacks on the strongest edges were most likely to degrade RI (Figs. 5(a) and 5(b)), which agreed with the high positive correlation between network density and RI (Fig. 2). Regarding the spatial embedding feature, the removal of the inter-hemispheric edges resulted in larger decrease in RI than deleting the intra-hemispheric ones (Figs. 5(c) and 5(d)).

C. Homotopic Edges: The Most Prominent Representatives of the "Resilience-Related" Edges

We observed that the total strength of some strongest edges had an inverted-U relationship with age. The goodness-of-fit (i.e., R-square value) rapidly increased with an increasing number of the strongest edges being taken into consideration in the beginning, then almost stabilized around 0.5 after a certain number (Fig. 6(a) and Supplementary Fig. S3). We caught the edges at the empirical saturation threshold 0.5 and found that the relationship between their strength and age could be well captured by the inverted-U shape curve. Since a similar relationship between RI and age was observed, intuitively, we speculated that these edges might be most relevant with resilience and referred them as 'resilience-related' edges for convenience.

We examined the spatial embedding feature of the 'resilience-related' edges, and found that the homotopic edges (i.e., edges that link two geometrically symmetrical regions) occurred most frequently among the 'resilience-related' edges, and the intra-hemispheric edges occurred the least frequently (Fig. 7 and Supplementary Fig. S3). This finding was further supported by an individual level analysis, where all edges were ranked according to their impacts on RI for each participant. Results showed that the homotopic edges had the highest average ranking for most participants (Fig. 8 and Supplementary Fig. S4). These results suggested that an arbitrary attack on the homotopic edges had the highest probability to degrade brain network resilience. Functional connectivity studies have demonstrated that the homotopic edges would be affected in stroke [59], [60], Alzheimer's disease [61], and Parkinson's disease [62], suggesting an abnormal functional integration and information communication. These discoveries would help support the applicability of RI in exploring the changes of brain resilience associated with disease.

The great influence of homotopic edges is not surprising given that they account for a high proportion in callosal fibers [63]. Corpus callosum has been reported to be affected in some neurodegenerative disorders including Alzheimer's disease and Dementia [64], [65]. Besides, branzoli and his colleagues pointed out that lower water fractional anisotropy in the corpus callosum could indicate the onset of demyelination processes with healthy aging [66]. The importance of human corpus callosum may be attributed to its significant role in large-scale bi-hemispheric integration [67], [68]. Alteration of the homotopic fiber tracts may disrupt the neural signal transmissions between two hemispheres and thus damage the functional homotopy (i.e., the functional synchrony between homotopic regions) [69]. Especially, homotopic functional edges has been reported to be critical in building brain intrinsic functional architecture [70]. Compared with concerns in functional homotopy, studies on homotopic structural edges are rare, which may be due to the sparseness of homotopic edges in the structural brain network (i.e., only a small number of homotopic edges in the structural brain network). Our results suggest that despite no dominance in number, structural homotopic edges may contribute most to brain network resilience.

V. Conclusion

This study assessed human brain resilience across the lifespan with a novel metric of network resilience, the Resilience Index (RI). The inverted-U lifespan trajectory between RI and age suggested that RI could be a candidate measure for brain resilience. Besides, we identified the vulnerable nodes like bi-hemisphere putamens and precuneus, and vulnerable edges (i.e., inter-hemispheric edges and edges with high strength). Specially, an arbitrary attack on homotopic edges would have a high probability to degrade brain network resilience. Our findings shed light on the intrinsic pattern of brain network resilience during development and aging and suggested that the Resilience Index may be applicable to identify vulnerable areas and edges, thus offering a new perspective to explore human brain vulnerability.

Acknowledgment

The first dataset was from the Cambridge Centre for Ageing and Neuroscience (Cam-CAN). Cam-CAN funding was provided by the U.K. Biotechnology and Biological Sciences Research Council under Grant BB/H008217/1, together with support from the U.K. Medical Research Council and the University of Cambridge, U.K. The authors appreciate the scientists working for Consortium for Reliability and Reproducibility (CoRR) and the enhanced Nathan Kline Institute-Rockland Sample (NKI-RS).

References

[1] N. A. Crossley *et al.*, "The hubs of the human connectome are generally implicated in the anatomy of brain disorders," *Brain*, vol. 137, no. 8, pp. 2382–2395, Aug. 2014.

[2] S. Achard, R. Salvador, B. Whitcher, J. Suckling, and E. Bullmore, "A resilient, low-frequency, small-world human brain functional network with highly connected association cortical hubs," *J. Neurosci.*, vol. 26, no. 1, pp. 63–72, Jan. 2006.

[3] B. Litt *et al.*, "Epileptic seizures may begin hours in advance of clinical onset: A report of five patients," *Neuron*, vol. 30, no. 1, pp. 51–64, Apr. 2001.

[4] Z. Yu *et al.*, "Altered brain anatomical networks and disturbed connection density in brain tumor patients revealed by diffusion tensor tractography," *Int. J. Comput. Assist. Radiol. Surg.*, vol. 11, no. 11, pp. 2007–2019, 2016.

[5] P. E. McSharry, L. A. Smith, and L. Tarassenko, "Prediction of epileptic seizures: Are nonlinear methods relevant?" *Nature Med.*, vol. 9, no. 3, pp. 241–242, Mar. 2003.

[6] J. G. Venegas *et al.*, "Self-organized patchiness in asthma as a prelude to catastrophic shifts," *Nature*, vol. 434, no. 7034, pp. 777–782, 2005.

[7] M. I. Falcon *et al.*, "The virtual brain: Modeling biological correlates of recovery after chronic stroke," *Frontiers Neurol.*, vol. 6, p. 228, Nov. 2015.

[8] S. R. Kesler, C. L. Watson, and D. W. Blayney, "Brain network alterations and vulnerability to simulated neurodegeneration in breast cancer," *Neurobiol. Aging*, vol. 36, no. 8, pp. 2429–2442, Aug. 2015.

[9] C. J. Stam, "Emergence of modular structure in a large-scale brain network with interactions between dynamics and connectivity," *Frontiers Comput. Neurosci.*, vol. 4, no. 1, pp. 231–236, 2010.

[10] O. Sporns, C. J. Honey, and R. Kötter, "Identification and classification of hubs in brain networks," *PLoS ONE*, vol. 2, no. 10, Oct. 2007, Art. no. e1049.

[11] O. Sporns, "The human connectome: A complex network," *Ann. New York Acad. Sci.*, vol. 1224, no. 1, pp. 109–125, Apr. 2011.

[12] K. W. Thee, H. Nisar, and C. S. Soh, "Graph theoretical analysis of functional brain networks in healthy subjects: Visual oddball paradigm," *IEEE Access*, vol. 6, pp. 64708–64727, 2018.

[13] C. J. Honey and O. Sporns, "Dynamical consequences of lesions in cortical networks," *Hum. Brain Mapping*, vol. 29, no. 7, pp. 802–809, Jul. 2008.

[14] M. P. Young, C. Hilgetag, and J. W. Scannell, "On imputing function to structure from the behavioural effects of brain lesions," *Phil. Trans. Roy. Soc. London. Ser. B, Biol. Sci.*, vol. 355, no. 1393, pp. 147–161, Jan. 2000.

[15] D. T. Rittman, M. R. Borchert, and M. S. Jones, "Functional network resilience to pathology in presymptomatic genetic frontotemporal dementia," *Neurobiol. Aging*, vol. 77, pp. 169–177, May 2019.

[16] F. váša, M. Shanahan, P. J. Hellyer, G. Scott, J. Cabral, and R. Leech, "Effects of lesions on synchrony and metastability in cortical networks," *NeuroImage*, vol. 118, pp. 456–467, Sep. 2015.

[17] J. Alstott, M. Breakspear, P. Hagmann, L. Cammoun, and O. Sporns, "Modeling the impact of lesions in the human brain," *PLoS Comput. Biol.*, vol. 5, no. 6, Jun. 2009, Art. no. e1000408.

[18] J. Cabral, M. L. Kringelbach, and G. Deco, "Functional connectivity dynamically evolves on multiple time-scales over a static structural connectome: Models and mechanisms," *NeuroImage*, vol. 160, pp. 84–96, Oct. 2017.

[19] J. Gao, B. Barzel, and A. L. Barabási, "Universal resilience patterns in complex networks," *Nature*, vol. 530, no. 7590, pp. 307–312, Feb. 2016.

[20] J. Liang, Y. Hu, G. Chen, and T. Zhou, "A universal indicator of critical state transitions in noisy complex networked systems," *Sci. Rep.*, vol. 7, no. 1, pp. 1–9, Mar. 2017.

[21] M. Barbier, J.-F. Arnoldi, G. Bunin, and M. Loreau, "Generic assembly patterns in complex ecological communities," *Proc. Nat. Acad. Sci. USA*, vol. 115, no. 9, pp. 2156–2161, Feb. 2018.

[22] E. Courchesne *et al.*, "Normal brain development and aging: Quantitative analysis at *in vivo* MR imaging in healthy volunteers," *Radiology*, vol. 216, no. 3, pp. 672–682, Sep. 2000.

[23] L. Nyberg, M. Lövdén, K. Riklund, U. Lindenberger, and L. Bäckman, "Memory aging and brain maintenance," *Trends Cognit. Sci.*, vol. 16, no. 5, pp. 292–305, May 2012.

[24] F. I. M. Craik and E. Bialystok, "Cognition through the lifespan: Mechanisms of change," *Trends Cognit. Sci.*, vol. 10, no. 3, pp. 131–138, Mar. 2006.

[25] G. Bartzokis, M. Beckson, P. H. Lu, K. H. Nuechterlein, N. Edwards, and J. Mintz, "Age-related changes in fronta and temporal lobe volumes in men: A magnetic resonance imaging study," *Arch. Gen. Psychiatry*, vol. 58, no. 5, pp. 461–465, 2001.

[26] T. Zhao *et al.*, "Age-related changes in the topological organization of the white matter structural connectome across the human lifespan," *Hum. Brain Mapping*, vol. 36, no. 10, pp. 3777–3792, 2015.

[27] J. R. Taylor *et al.*, "The Cambridge centre for ageing and neuroscience (Cam-CAN) data repository: Structural and functional MRI, MEG, and cognitive data from a cross-sectional adult lifespan sample," *NeuroImage*, vol. 144, pp. 262–269, Jan. 2017.

[28] X. N. Zuo *et al.*, "An open science resource for establishing reliability and reproducibility in functional connectomics," *Sci. Data*, vol. 1, no. 1, pp. 1–13, 2014.

[29] K. B. Nooner *et al.*, "The NKI-rockland sample: A model for accelerating the pace of discovery science in psychiatry," *Frontiers Neurosci.*, vol. 6, p. 152, Oct. 2012.

[30] Z. Cui, S. Zhong, P. Xu, Y. He, and G. Gong, "PANDA: A pipeline toolbox for analyzing brain diffusion images," *Frontiers Human Neurosci.*, vol. 7, p. 42, Feb. 2013.

[31] A. Leemans and D. K. Jones, "The B-matrix must be rotated when correcting for subject motion in DTI data," *Magn. Reson. Med.*, vol. 61, no. 6, pp. 1336–1349, Jun. 2009.

[32] W. H. Jung, S. Lee, C. Lerman, and J. W. Kable, "Amygdala functional and structural connectivity predicts individual risk tolerance," *Neuron*, vol. 98, no. 2, pp. 394–404, 2018.

[33] R. Fang *et al.*, "Disrupted structural brain network in AD and aMCI: A finding of long fiber degeneration," *Current Alzheimer Res.*, vol. 12, no. 6, pp. 572–584, Jul. 2015.

[34] Y. Sun *et al.*, "Disrupted functional brain connectivity and its association to structural connectivity in amnestic mild cognitive impairment and Alzheimer's disease," *PLoS ONE*, vol. 9, no. 5, May 2014, Art. no. e96505.

[35] D. Clewett, S. Bachman, and M. Mather, "Age-related reduced prefrontal-amygdala structural connectivity is associated with lower trait anxiety," *Neuropsychology*, vol. 28, no. 4, pp. 631–642, 2014.

[36] T. Zhao, C. Sheng, Q. Bi, W. Niu, N. Shu, and Y. Han, "Age-related differences in the topological efficiency of the brain structural connectome in amnestic mild cognitive impairment," *Neurobiol. Aging*, vol. 59, pp. 144–155, Nov. 2017.

[37] R. M. May, "Thresholds and breakpoints in ecosystems with a multiplicity of stable states," *Nature*, vol. 269, no. 5628, pp. 471–477, Oct. 1977.

[38] A. M. Lyapunov, "The general problem of the stability of motion," *Int. J. Control*, vol. 55, no. 3, pp. 531–534, 1992.

[39] C.-C. Huang *et al.*, "Nonlinear pattern of the emergence of white matter hyperintensity in healthy Han Chinese: An adult lifespan study," *Neurobiol. Aging*, vol. 67, pp. 99–107, Jul. 2018.

[40] G. Bartzokis, D. Sultzer, P. H. Lu, K. H. Nuechterlein, J. Mintz, and J. L. Cummings, "Heterogeneous age-related breakdown of white matter structural integrity: Implications for cortical 'disconnection' in aging and Alzheimer's disease," *Neurobiol. Aging*, vol. 25, no. 7, pp. 843–851, Aug. 2004.

[41] M. Rubinov and O. Sporns, "Complex network measures of brain connectivity: Uses and interpretations," *NeuroImage*, vol. 52, no. 3, pp. 1059–1069, 2010.

[42] L. Wilkinson and M. Friendly, "The history of the cluster heat map," *Amer. Statistician*, vol. 63, no. 2, pp. 179–184, May 2009.

[43] A. Menardi, A. E. Reineberg, A. Vallesi, N. P. Friedman, M. T. Banich, and E. Santarnecchi, "Heritability of brain resilience to perturbation in humans," *NeuroImage*, vol. 235, Jul. 2021, Art. no. 118013.

[44] B. R. Scheffers *et al.*, "The broad footprint of climate change from genes to biomes to people," *Science*, vol. 354, no. 6313, Nov. 2016, Art. no. aaf7671.

[45] A. Testolin and M. Zorzi, "Probabilistic models and generative neural networks: Towards an unified framework for modeling normal and impaired neurocognitive functions," *Frontiers Comput. Neurosci.*, vol. 10, p. 73, Jul. 2016.

[46] L. Fan *et al.*, "The human brainnetome atlas: A new brain atlas based on connectional architecture," *Cerebral Cortex*, vol. 26, no. 8, pp. 3508–3526, 2016.

[47] D. Yin *et al.*, "Dissociable changes of frontal and parietal cortices in inherent functional flexibility across the human life span," *J. Neurosci.*, vol. 36, no. 39, pp. 10060–10074, Sep. 2016.

[48] F. G. Hillary and J. H. Grafman, "Injured brains and adaptive networks: The benefits and costs of hyperconnectivity," *Trends Cognit. Sci.*, vol. 21, no. 5, pp. 385–401, May 2017.

[49] E. Santarnecchi, S. Rossi, and A. Rossi, "The smarter, the stronger: Intelligence level correlates with brain resilience to systematic insults," *Cortex*, vol. 64, pp. 293–309, Mar. 2015.
[50] L. D. F. Costa, F. A. Rodrigues, G. Travieso, and P. R. V. Boas, "Characterization of complex networks: A survey of measurements," *Adv. Phys.*, vol. 56, no. 1, pp. 167–242, Jan. 2007.
[51] G. Gong, P. Rosa-Neto, F. Carbonell, Z. J. Chen, Y. He, and A. C. Evans, "Age- and gender-related differences in the cortical anatomical network," *J. Neurosci.*, vol. 29, no. 50, pp. 15684–15693, Dec. 2009.
[52] Y. Iturria-Medina, R. C. Sotero, E. J. Canales-Rodríguez, Y. Alemán-Gómez, and L. Melie-García, "Studying the human brain anatomical network via diffusion-weighted MRI and graph theory," *NeuroImage*, vol. 40, no. 3, pp. 1064–1076, Apr. 2008.
[53] M. P. van den Heuvel and O. Sporns, "Rich-club organization of the human connectome," *J. Neurosci.*, vol. 31, no. 44, pp. 15775–15786, 2011.
[54] C. O'Callaghan, M. Bertoux, and M. Hornberger, "Beyond and below the cortex: The contribution of striatal dysfunction to cognition and behaviour in neurodegeneration," *J. Neurol., Neurosurg. Psychiatry*, vol. 85, no. 4, pp. 371–378, Apr. 2014.
[55] A. V. Utevsky, D. V. Smith, and S. A. Huettel, "Precuneus is a functional core of the default-mode network," *J. Neurosci.*, vol. 34, no. 3, pp. 932–940, Jan. 2014.
[56] W. A. Chaovalitwongse *et al.*, "Network optimization of functional connectivity within default mode network regions to detect cognitive decline," *IEEE Trans. Neural Syst. Rehabil. Eng.*, vol. 25, no. 7, pp. 1079–1089, Jul. 2017.
[57] P. T. Bell and J. M. Shine, "Subcortical contributions to large-scale network communication," *Neurosci. Biobehav. Rev.*, vol. 71, pp. 313–322, Dec. 2016.
[58] K. Kantarci *et al.*, "White-matter integrity on DTI and the pathologic staging of Alzheimer's disease," *Neurobiol. Aging*, vol. 56, pp. 172–179, Aug. 2017.
[59] J. S. Siegel *et al.*, "Disruptions of network connectivity predict impairment in multiple behavioral domains after stroke," *Proc. Nat. Acad. Sci. USA*, vol. 113, no. 30, pp. E4367–E4376, Jul. 2016.
[60] M. Corbetta, J. S. Siegel, and G. L. Shulman, "On the low dimensionality of behavioral deficits and alterations of brain network connectivity after focal injury," *Cortex*, vol. 107, pp. 229–237, Oct. 2018.
[61] G. Chen *et al.*, "Modular reorganization of brain resting state networks and its independent validation in Alzheimer's disease patients," *Frontiers Human Neurosci.*, vol. 7, p. 456, Aug. 2013.
[62] J. Li *et al.*, "Decreased interhemispheric homotopic connectivity in Parkinson's disease patients with freezing of gait: A resting state fMRI study," *Parkinsonism Rel. Disorders*, vol. 52, pp. 30–36, Jul. 2018.
[63] G. M. Innocenti, "General organization of callosal connections in the cerebral cortex," in *Sensory-Motor Areas and Aspects of Cortical Connectivity*, E. G. Jones and A. Peters, Eds. Boston, MA, USA: Springer, 1986, pp. 291–353, doi: 10.1007/978-1-4613-2149-1_9.
[64] R. N. Køster, R. Jesper, and P. Bente, "The total number of myelinated nerve fibers is reduced in corpus callosum in brains from patients with Alzheimer's disease," *Neurobiol. Aging*, vol. 69, pp. 58–64, Sep. 2018.
[65] J. Yu and T. M. C. Lee, "The longitudinal decline of white matter microstructural integrity in behavioral variant frontotemporal dementia and its association with executive function," *Neurobiol. Aging*, vol. 76, pp. 62–70, Apr. 2019.
[66] F. Branzoli *et al.*, "Differentiating between axonal damage and demyelination in healthy aging by combining diffusion-tensor imaging and diffusion-weighted spectroscopy in the human corpus callosum at 7 T," *Neurobiol. Aging*, vol. 47, pp. 210–217, Nov. 2016.
[67] E. Luders, P. M. Thompson, and A. W. Toga, "The development of the corpus callosum in the healthy human brain," *J. Neurosci.*, vol. 30, no. 33, pp. 10985–10990, Aug. 2010.
[68] C. Ryberg *et al.*, "Clinical significance of corpus callosum atrophy in a mixed elderly population," *Neurobiol. Aging*, vol. 28, no. 6, pp. 955–963, Jun. 2007.
[69] R. Gasparotti *et al.*, "Reduced fractional anisotropy of corpus callosum in first-contact, antipsychotic drug-naive patients with schizophrenia," *Schizophrenia Res.*, vol. 108, nos. 1–3, pp. 41–48, Mar. 2009.
[70] R. Salvador *et al.*, "A simple view of the brain through a frequency-specific functional connectivity measure," *NeuroImage*, vol. 39, no. 1, pp. 279–289, Jan. 2008.